Transients in porous media: asymptotic time-domain Green functions and limits of current frequency-domain models

Jean Kergomard, Denis Lafarge, Joël Gilbert

Transients in porous media: asymptotic time-domain Green functions and limits of current frequency-domain models

J. Kergomard*(a), D. Lafarge (b), J. Gilbert (b)

(a) LMA, CNRS, UPR 7051, Aix-Marseille Univ, Centrale Marseille, F-13402 Marseille Cedex 20, France
(b) LUNAM Université, Université du Maine, ¡CNRS UMR 6613¿, Laboratoire d'Acoustique, Avenue Olivier Messiaen, 72085 LE MANS CEDEX 9, France.

May 16, 2012

Abstract

Time domain responses of porous media have been studied by some authors, but generally the possible descriptions have been given in the frequency domain. The aim of this paper, limited to materials with rigid skeleton considered as equivalent fluids, is to compare the descriptions by Johnson-Allard (JA) as well as by Pride-Lafarge (PL) with i) some analytical, approximate formulas, based upon asymptotic high frequency expansion ; ii) the exact formula by Zwikker and Kosten for the case of cylindrical pores. The paper starts with a short summary of the statement of the different general full frequency models (JA and PL). The Green function in the time domain is shown to exhibit interesting properties of materials. In particular the maximum response depends on one dimensionless parameter only, which is denoted ξ and is the ratio of the travelled distance to the product of the "frozen" sound speed and a characteristic viscous relaxation time. The distance ξ is related to a time domain Stokes number. The numerical computation of the Green function is done by FFT, with some precautions, because of the importance of the higher frequencies on the response shape. The PL description is shown to be the best full frequency general model, but some discrepancies with the exact model appear at short times or short distances. When the distance ξ increases from zero, the asymptotic expansion shows that the maximum of the Green function decreases first as $1/\xi^2$, then exponentially.

Keywords: Pulse propagation; Transient signals; Porous material

PACS: 43.55 Rv, 43.55 Ti, 43.20 Gp, 43.20 Bi, 43.20 Hq

*Tel 33 491164381, Fax 33 491228248, kergomard@lma.cnrs-mrs.fr

1 Introduction

Long-wavelength wave propagation in homogeneous porous media is a classical topic. In particular for materials with a rigid skeleton considered as equivalent fluids, the classical homogenization theory gives us recipes to compute the complex, frequency-dependent, equivalent-fluid density and compressibility. This computation would require knowing, however, the detailed microgeometry of the solid. In absence of this knowledge, a widely used 1D semi phenomenological frequency-domain model of propagation which depends on a small set of geometrical parameters of the structure is given by the well-known formula of Johnson et al. [1] for the density, and the Champoux-Allard [10] or Lafarge et al. [9] formulae for the compressibility. These approximate expressions (denoted JA) of the two constitutive functions essentially are the result of:

1) a relatively precise description of the high-frequency limit, the two first leading terms of the two functions, density and compressibility, being exactly described in terms of the concepts of ideal-fluid tortuosity α_∞ and characteristic lengths Λ (see Ref. [1]) and Λ' (see Ref. [10]), the viscous and thermal relaxation processes being "frozen" in this limit,

2) a less precise description of the low-frequency limit, only the first nontrivial leading term of the two functions being exactly described in terms of the concepts of d.c. viscous and thermal permeabilities, k_0 (see Ref. [4]) and k'_0 (see Refs. [9, 12]), the viscous and thermal relaxation processes being "relaxed" in this limit, and finally,

3) an assumption that the frozen and relaxed limits 1) and 2) are connected in the simplest authorized manner, i.e. (see [1] and [9, 12]), by means of the simplest functions of frequency ω having their singularities and zeros lying on the imaginary axis (in the complex ω plane). Indeed, this assumption is equivalent to stating that the fluid velocity pattern at the pore scale is divergence-free, and this characteristics of the fluid motion tends to be verified (at least, as long as the geometry remains sufficiently simple) as a result of the long-wavelength separation condition which ensures that a homogenized medium exists.

In this manner, a simple, resp. viscous and thermal, relaxation-transition description of the density and compressibility functions is obtained, that may be thought to be well-verified in a wide class of materials, as long as the wavelengths are large compared to the typical dimensions of the coarse-graining averaging volumes.

Subsequently, the low-frequency relaxed limit 2) was made more precise by Pride et al. [11] and Lafarge [12] (the next viscous and nontrivial thermal terms now being exactly described thanks to the introduction of the additional notions of d.c. viscous and thermal tortuosities α_0 and α'_0), resulting in a slightly improved (denoted PL) description of the relaxation transitions of the two functions.

In Ref. [13], Fellah et al. concentrated on the time-domain expression of the high-frequencies asymptotics implied by this model.

Expanding, in the high-frequency limit, the PL density and compressibility in powers of the inverse Stokes number St^{-1} (defined as the ratio between boundary layer thickness and characteristic pore size), and retaining the (exact) zero and first order terms and the (model-dependent) second order terms, they derived an asymptotic time-domain pressure wave equation. Using fractional-

derivative and Laplace-transform calculus, they were able to rigorously solve this equation in instructive and elegant manner, through the calculation of the corresponding asymptotic Green function of the unbounded 1D medium. Recall that a Green function or impulse response, as a function of time, extends and flattens when observed at fixed locations more and more remote from the spatial point where it originates. Like the wave equation used to construct it, however, the above asymptotic Green function was (partly) model dependent.

Now, the results of the calculations made in [13] seem to indicate that the terms of second order yield a significant effect on the Green function for resistive porous materials, and, in addition, that the effect is mainly an effect on the amplitude without noticeable distortion of the time wave pattern (see Figs. 2 and 3 of paper [13]).

In the present paper, our purpose is threefold.

First, paying attention to distinguish between the results that are general and the results that are model-dependent, we shall justify in another simple alternative analytic manner the finding of Ref. [13] summarized above. Indeed, by exploiting the model-independent fact that (with some restrictions on the geometry) the high-frequency asymptotic expansion of the wavenumber expands in successive powers of St^{-1}, and considering the $o(2)$ expansion, we shall obtain a closed-form expression of a corresponding asymptotic time-domain Green function $G_{o(2)}(x,t)$. Exactly the same closed-form expression was obtained before by Polack et al. [18] for the special case of cylindrical circular tubes. Therefore, like this special one, our general asymptotic $o(2)$ Green function differs from the asymptotic $o(1)$ one only by an amplitude factor $\exp(-C_\omega x)$ independent of time: $G_{o(2)}(x,t) = G_{o(1)}(x,t)\exp(-C_\omega x)$. This is the above-mentioned second-order attenuation with no distortion effect.

Next, we hasten to point out that by construction, the models PL and JA unfortunately yield faulty values for the coefficient C_ω involved, and hence, faulty descriptions of this asymptotic second order attenuation effect.

Finally, we try to assess in which circumstances this want of precision of the models PL and JA is manifested on the Green functions. To this end, we make detailed comparisons between the modeled and exact Green functions, computed by FFT, for the case of cylindrical circular pores. Recall that for this geometry, exact results exist since Zwikker and Kosten [14], in frequency-domain, for the effective density and compressibility. It appears that the lack of precision of existing models is manifested mainly at sufficiently "short" propagation distances x (past the spatial origin $x = 0$ of the impressed impulsive signal) and sufficiently "long" delayed times $t-x/c$ (meaning the times t elapsed past the first arrival time x/c of the signal, with $c = c_f/\sqrt{\alpha_\infty}$ the frozen speed of sound in the medium and c_f the speed of sound in the fluid). In terms of the dimensionless distances $\xi = x/c\Theta$ and delayed times $\tau = (t-x/c)/\Theta$, where Θ is a characteristic relaxation time (varying like the square of the pore size divided by the fluid kinematic viscosity), this means a limited region of the plane (ξ, τ) near the origin. Outside this region i.e. at sufficiently "large" propagation distances x and/or delayed arrival times $t - x/c$ (where "large" is inversely proportional, for a given shape of the pores, to the flow resistivity of the material), the existing models and especially PL, perform quite well.

The paper is organized as follows.

After the statement of the basic equations (section 2), the high-frequencies asymptotic wave equation and wave number are written (section 3 and 4), re-

taining terms of order $O(2)$ (i.e. $\sim St^{-2}$). As anticipated on general grounds, it is explicitly checked on the workable case of cylindrical circular pores, that the latter terms are not accurately described by the models JA and PL (section 2). Using $o(1)$ and $o(2)$ asymptotic expansions of the wavenumber, two corresponding asymptotic Green functions in the time domain are derived (section 4). These are the direct transposition of those given in [18] for the case of cylindrical circular tubes. By construction, our time domain $o(2)$ Green function is obtained at the same order of accuracy as that derived in [13]. The evaluation, by FFT, of all different time-domain Green's functions based on exact or approximate frequency-domain expressions, is discussed in section 5. The behaviors of the different expressions are compared and contrasted in section 6, in particular for the entirely workable case of cylindrical circular pores.

2 Basic equations

We start by recalling the form of the macroscopic Equivalent-fluid equations in the frequency domain (see [1, 9, 19]):

$$\rho_f \alpha(\omega) i\omega v_i = \nabla_i p \;\; ; \;\; K_a^{-1} \beta(\omega) i\omega p = \boldsymbol{\nabla}.v \;, \tag{1}$$

where by definition, $\mathbf{v}$ and p are the macroscopic velocity and pressure obtained by coarse-graining (averaging) the microscopic fluid velocity and pressure fields, $-i\omega$ is the time derivative, ρ_f and K_a are the saturating-fluid density and adiabatic bulk modulus, and $\alpha(\omega)$ and $\beta(\omega)$ are the dynamic tortuosity and the dynamic compressibility. Notice that for simplicity, isotropy or 1D propagation along one principal axis is assumed, so that $\alpha(\omega)$ is a scalar.

As every macroscopic theory, the Equivalent-fluid theory assumes a long-wavelength regime, i.e. a wide separation between the macroscopic wavelength and the typical porous medium lengthscale involved in obtaining the coarse-grained macroscopic variables. Now, the special form of Eqs. (1) shows that the theory assumes much more than this. Indeed, as only the frequencies and not the wavenumbers are apparent in Eqs. (1), it appears that the Equivalent-fluid theory is certainly a simplified macroscopic description limited to describe the situations in which only the temporal dispersion – and not the spatial dispersion – effects are important [21]. Allowing for the spatial dispersion effects will lie outside the framework and scope of this paper.

Coherent with this physical simplification which is well-justified in most geometries (the condition to neglect spatial dispersion is certainly the same as that which allows us stating that the fluid velocity pattern tends to be divergence-free at the pore scale) an application of the homogenization technique [9] at order zero yields two different microscopic boundary value formal problems to be solved for determining the two constitutive functions $\alpha(\omega)$ and $\beta(\omega)$.

The first one describes the (velocity) response of a viscous incompressible fluid subject to an applied spatially uniform, time harmonic, bulk force source term:

$$\frac{-i\omega\rho_f}{\eta}\mathbf{w} = -\boldsymbol{\nabla}\Pi + \boldsymbol{\nabla}^2\mathbf{w} + \mathbf{e}, \tag{2}$$

$$\boldsymbol{\nabla}\cdot\mathbf{w} = 0, \tag{3}$$

in the pore space (with Π a periodic or stationary random field, in periodic or stationary random geometries), and satisfying on the pore surface (no slip condition),

$$\mathbf{w} = \mathbf{0}. \tag{4}$$

In this problem, η is the fluid viscosity, $\mathbf{e}$ is a dimensionless unit vector in the direction of the applied bulk force, and $\mathbf{w}$ is the scaled response velocity field (dimension of $length^2$). It determines the dynamic permeability $k(\omega)$ and dynamic tortuosity $\alpha(\omega)$ introduced in the landmark paper by Johnson et al. [1], by the relations:

$$k(\omega) = \frac{\eta\phi}{-i\omega\rho_f\alpha(\omega)} = \langle \mathbf{w} \rangle \cdot \mathbf{e}, \tag{5}$$

where $\langle\rangle$ is the coarse-graining averaging operation in the pore space, and ϕ is the porosity.

The other describes the (excess temperature) response of a thermal fluid subject to an applied spatially uniform, time harmonic, pressure source term:

$$\frac{-i\omega \Pr \rho_f}{\eta}\theta = \boldsymbol{\nabla}^2\theta + 1, \tag{6}$$

in the pore space, and satisfying on the pore surface (no temperature-jump condition),

$$\theta = 0. \tag{7}$$

Here, 1 is a dimensionless unit constant representing the applied pressure, Pr is the Prandtl number, and θ is the scaled response excess temperature field (dimension of $length^2$). It determines the functions $k'(\omega)$ and $\alpha'(\omega)$, thermal counterparts of functions $k(\omega)$ and $\alpha(\omega)$ introduced by Lafarge [9,12], and then, the effective compressibility $\beta(\omega)$, by the following relationships:

$$k'(\omega) = \frac{\eta\phi}{-i\omega \Pr \rho_f\alpha'(\omega)} = \langle\theta\rangle \quad ; \quad \beta(\omega) = \gamma - \frac{\gamma - 1}{\alpha'(\omega)}. \tag{8}$$

2.1 Frozen and relaxed limits

In absence of a complete information on the microgeometry, the two above-mentioned microscopic formal boundary-value problems cannot entirely be worked out and their exact detailed solutions (from which $\alpha(\omega)$ and $\beta(\omega)$ can in principle be extracted by coarse-graining, see Eqs.(5) and (8)) are missing. Nevertheless, tacit, hidden, but very important assumptions on the geometry have been made in obtaining these problems (namely, that it is possible to neglect spatial dispersion), and these assumptions have had the consequence that in the first problem the stirring force $\mathbf{e}$ was set constant (and accordingly the velocity field $\mathbf{v}$ was represented by a divergence-free field), and in the second problem the stirring pressure term 1 was set constant (gradient-free). We shall later indicate what exactly mean these two characteristics of the obtained problems: they mean that the functions $\alpha(\omega)$ and $\alpha'(\omega)$ have purely imaginary singularities and thus are relatively smooth functions on the real axis (this is property 3 mentioned in Introduction). For the time being, we observe that in the limit of high-frequencies and low-frequencies, which we may call the frozen and relaxed, respectively, limits of the viscous and thermal relaxation processes involved, some general

characteristics of the solutions and corresponding functions $\alpha(\omega)$ and $\beta(\omega)$ may be sketched as follows.

2.1.1 High frequencies (frozen limit)

In the asymptotic frozen limit of high frequencies, the viscous and thermal terms $\boldsymbol{\nabla}^2\mathbf{w}$ and $\boldsymbol{\nabla}^2\theta$ become negligibly small compared to the other terms. The fluid motions, except for vanishingly small viscous and thermal boundary layers at the pore walls, become close to those of an inviscid nonconducting fluid ($\eta = 0, \kappa = 0$, κ is the thermal conductivity). Accordingly, the quantities $\frac{-i\omega\rho_f}{\eta}\mathbf{w}$ and $\frac{-i\omega\,\mathrm{Pr}\,\rho_f}{\eta}\theta$ everywhere tend (except, of course, at the pore walls) to the "frozen" fields $\mathbf{E}$ and I verifying in the pore space, (with φ a periodic or stationary random field, in periodic or stationary random geometries),

$$\begin{aligned} \mathbf{E} &= -\boldsymbol{\nabla}\varphi + \mathbf{e} \;\; ; \;\; I = 1, & (9)\\ \boldsymbol{\nabla}\cdot\mathbf{E} &= 0, & (10) \end{aligned}$$

and verifying at the pore walls ($\mathbf{n}$ is the normal on the latter),

$$\mathbf{E}\cdot\mathbf{n} = \mathbf{0}. \tag{11}$$

Now assume, following Johnson et al. [1] and Allard [8], that the pore-surface interface appears locally plane in this asymptotic high-frequency frozen limit. This is an assumption that the viscous and thermal boundary layer thicknesses $\delta = \sqrt{\frac{2\eta}{\rho_f\omega}}$ and $\delta' = \sqrt{\frac{2\eta}{\rho_f\omega\,\mathrm{Pr}}}$ eventually become small compared to a characteristic radius of curvature of the pore surface. Then, the functions $\alpha(\omega)$ and $\alpha'(\omega)$ expand in integral power series of these thicknesses, which allows us writing a priori[1],

$$\begin{aligned} \alpha(\omega) &= \alpha_\infty + \frac{2\alpha_\infty}{\Lambda}\left(\frac{\eta}{-i\omega\rho_f}\right)^{1/2} + O\left(\frac{1}{-i\omega}\right) \;\; ; \\ \alpha'(\omega) &= \alpha'_\infty + \frac{2\alpha'_\infty}{\Lambda'}\left(\frac{\eta}{-i\omega\rho_f\,\mathrm{Pr}}\right)^{1/2} + O\left(\frac{1}{-i\omega}\right). \end{aligned} \tag{12}$$

The intervening geometrical parameters α_∞ and α'_∞ (dimensionless) and Λ and Λ' (dimension of *length*) must be some pore averages constructed with the frozen fields $\mathbf{E}$ and I. Indeed, detailed classic calculations made by Johnson and Allard [1, 10], to which we refer the reader, show that they may be written as follows (see also [19] and, in the most detailed manner for Λ, [5]):

$$\frac{1}{\alpha_\infty} = \langle\mathbf{E}\rangle\cdot\mathbf{e} = \frac{\langle\mathbf{E}\rangle^2}{\langle\mathbf{E}^2\rangle} \;\; ; \;\; \frac{1}{\alpha'_\infty} = \langle\mathbf{I}\rangle = 1, \tag{13}$$

[1]Notice that the case of fractal geometry which modifies the exponent 1/2 in the first correction terms – see [1] – is excluded by the assumption that the pore walls appear locally flat at the scale of the boundary layer thickness; the presence of sharp edges which modifies the exponent 1 in the second correction terms – see [5] – is also excluded by this assumption.

and,

$$\frac{2}{\Lambda} = \frac{\int_{S_p} \mathbf{E}^2 dS}{\int_{V_f} \mathbf{E}^2 dV} \;\; ; \;\; \frac{2}{\Lambda'} = \frac{\int_{S_p} I^2 dS}{\int_{V_f} I^2 dV} = \frac{\int_{S_p} dS}{\int_{V_f} dV} \;\; , \tag{14}$$

where S_p denotes the pore walls and V_f denotes the connected pore volume.

Parameter Λ is an effective pore radius for dynamically connected pore sizes which was introduced by Johnson et al. [2] for the problem of electrical conduction in the bulk fluid, perturbed by a thin, different conducting layer at the pore walls. Parameter Λ' is a length characterizing a simpler effective pore radius – twice the fluid-volume to fluid-surface ratio – sometimes referred to as the Kozeny-Carman radius; Allard [10], inspired by Johnson's identification of the tortuosity high-frequency frozen limit, identified it as the thermal counterpart of parameter Λ. Mention that an erroneous expression for Λ was sometimes employed [3]; the reasoning inaccuracy[2] was clarified and corrected in [5] along a line tentatively sketched in [6] (Appendix D).

2.1.2 Low frequencies (relaxed limit)

In the opposite relaxed limit of low frequencies, the viscous and thermal terms $\boldsymbol{\nabla}^2\mathbf{w}$ and $\boldsymbol{\nabla}^2\theta$ eventually become much greater than the inertial terms $\frac{-i\omega\rho_f}{\eta}\mathbf{w}$ and $\frac{-i\omega \Pr \rho_f}{\eta}\theta$ and the boundary layers extend to the whole fluid. Accordingly, the fields $\mathbf{w}$ and θ everywhere tend to the d.c. – or "relaxed" – velocity and excess temperature fields $\mathbf{w}_0$ and θ_0 verifying, in the pore space (with Π_0 a periodic or stationary random field, in periodic or stationary random geometries),

$$\boldsymbol{\nabla}^2\mathbf{w}_0 = \boldsymbol{\nabla}\Pi_0 - \mathbf{e} \;\; ; \;\; \boldsymbol{\nabla}^2\theta_0 = -1, \tag{15}$$

$$\boldsymbol{\nabla}\cdot\mathbf{w}_0 = 0. \tag{16}$$

and verifying, at the pore walls,

$$\mathbf{w}_0 = \mathbf{0} \;\; ; \;\; \theta_0 = 0.$$

In this limit the functions $\alpha(\omega)$ and $\alpha'(\omega)$ expand in Laurent's series,

$$\alpha(\omega) = \frac{\eta\phi}{-i\omega\rho_f k_0} + \alpha_0 + O(-i\omega) \;\; ; \;\; \alpha'(\omega) = \frac{\eta\phi}{-i\omega\rho_f \Pr k_0'} + \alpha_0' + O(-i\omega). \tag{17}$$

The two first intervening geometrical parameters, k_0 (Darcy's viscous permeability) and k_0' (its thermal counterpart [9,12]) on one hand, both having dimension of $length^2$, and α_0 (viscous tortuosity) and α_0' (its thermal counterpart) on the other hand, both being dimensionless, are pore averages constructed with the relaxed fields $\mathbf{w}_0$ and θ_0. Indeed, simple calculations show that they may be

[2]The ignorance, in the bulk, i.e. outside the viscous boundary layer or the perturbed conducting layer, of a perturbation contribution due to a perturbed ideal-fluid or electrical bulk flow field orthogonal to the leading bulk flow field $\mathbf{E}$, and having, contrary to the latter, nonzero normal components at the pore walls.

written ([7, 12]),

$$k_0 = \phi \langle \mathbf{w}_0 \rangle \cdot \mathbf{e} \ ; \ k_0' = \phi \langle \theta_0 \rangle , \tag{18}$$

$$\alpha_0 = \frac{\langle \mathbf{w}_0^2 \rangle}{\langle \mathbf{w}_0 \rangle^2} \ ; \ \alpha_0' = \frac{\langle \theta_0^2 \rangle}{\langle \theta_0 \rangle^2}. \tag{19}$$

Mention that, among other things it is possible to show that, whatever the geometry,

$$\alpha_0 > \alpha_\infty \geq 1, \tag{20}$$

$$k_0 \leq k_0' \ ; \ \alpha_0 \geq \alpha_0' \ ; \ \Lambda \leq \Lambda', \tag{21}$$

the equalities being satisfied only for the case of aligned cylindrical pores.

2.2 Full-frequency models

Let us now come back to our hypothesis that spatial dispersion is absent. This hypothesis is an assumption that the geometry is sufficiently simple not to have structures such as Helmholtz resonators manifesting the presence of widely different pore sizes (the resonator neck and cavity dimensions). It is in absence of such structures and effects that the long-wavelength separation condition ensures that the microscopic flow-field may be considered divergence-free for the purpose of determining the microscopic fluid velocity pattern (see Eq. (3)), and likewise, the excess pressure field may be considered gradient-free for the purpose of determining the microscopic excess temperature pattern.

Now, Johnson et al. have shown that, because the velocity field may be viewed locally divergence-free, the singularities of functions $\alpha(\omega)$ and $k(\omega)$ – poles, zeros, and branch points – necessarily are purely imaginary (see [1] Appendix A). This also was shown by Avellaneda and Torquato [6]: assuming periodicity, a formal solution of the problem (2-4) directly expresses in temporal domain, in terms of a distribution of relaxation times.

For the functions $\alpha'(\omega)$ and $k'(\omega)$, it was similarly shown that, because the excess pressure field may be considered gradient-free, the singularities of functions $\alpha'(\omega)$ and $k'(\omega)$ also are purely imaginary (see [9] Appendix C).

The wanted functions must therefore have very simple and smooth behaviors on the real axis. For example, calculations [12] inspired by the DRT formalism of Avellaneda and Torquato show that in the Laplace domain ($s = -i\omega > 0$) the permeability function $k(s)$ is always a strictly decreasing positive function on the real axis $s > 0$ (and the same holds true in the same manner for the thermal permeability function $k'(s)$).

Finally, as suggested by Johnson et al., the functions $k(\omega)$ and $\alpha(\omega)$, as well as the functions $k'(\omega)$ and $\alpha'(\omega)$, will be seeked as the simplest ones, satisfying both the frozen and relaxed limits and the condition that they have purely imaginary singularities.

To proceed, let us introduce a Stokes number constructed using Johnson's concept of dynamically connected pore size Λ, viz:

$$St = \Lambda \sqrt{\frac{-i\omega\rho_f}{\eta}}. \tag{22}$$

Johnson has proposed the following expression of $\alpha(\omega)$,

$$\alpha(\omega) = \alpha_\infty \left(1 + \frac{8}{MSt^2} \sqrt{1 + \frac{M^2}{16} St^2} \right), \tag{23}$$

where

$$M = \frac{8\alpha_\infty k_0}{\phi \Lambda^2} \tag{24}$$

is a dimensionless shape factor associated to the geometry. This expression is the simplest analytical ansatz that yields the exact first two terms at high frequencies (Eq. (12)) and the exact first leading term at low frequencies (Eq.((17)), and automatically satisfies the condition on singularities. Factor of 8 is introduced for convenience in Eq. (24), so that $M = 1$ for cylindrical circular pores.

Similarly, to describe the function $\alpha'(\omega)$ let us introduce a second Stokes number corresponding to thermal effects:

$$St' = \Lambda' \sqrt{\frac{-i\omega\rho_f \, \mathrm{Pr}}{\eta}}. \tag{25}$$

The ratio $St'/St = \sqrt{\mathrm{Pr}}\ \Lambda'/\Lambda$ is of the order of $\mathrm{Pr}^{1/2}$, not far from unity. Proceeding as did Johnson, Lafarge [12] proposed to write,

$$\alpha'(\omega) = 1 + \frac{8}{M' St'^2} \sqrt{1 + \frac{M'^2}{16} St'^2}, \tag{26}$$

where

$$M' = \frac{8k_0'}{\phi \Lambda'^2} \tag{27}$$

is the thermal counterpart of shape factor M ($M' = 1$ for cylindrical circular pores), giving in turn a definite model for the dynamic compressibility

$$\beta(\omega) = \gamma - (\gamma - 1)/\alpha'(\omega). \tag{28}$$

As one key recognition of this model – namely, that there is one length Λ' playing for thermal effects the role of Johnson's Λ for viscous effects – was due to Allard [10], we refer to the combined modeling of functions α and β as to Johnson-Allard's (JA).

Subsequently, Pride et al. [11], studying oscillating viscous flow in convergent-divergent channels, evidenced the fact that Johnson's simple formula (23) (as was already anticipated in [1]) may significantly underestimate the imaginary part of permeability at low frequencies. To remedy this, they proposed different modifications of the formula. In essence these modifications produce formulae capable to account for the exact value of parameter α_0, which, in such channels, may be significantly increased as compared to Johnson's. Notwithstanding, focusing on the imaginary part of the permeability, they did not use and mention the parameter α_0. Its identification (see Eq. (19)) shows that it is a measure of "disorder" of the "Poiseuille" flow in the given microgeometry, so that it is increased not only by the convergent-divergent mechanism considered by Pride et al., but also, e.g., by the effect of a mere irregular distribution of solid inclu-

sions. Whatever the cause of the enhanced "Poiseuille disorder", it will make more significant the use of the Pride modified formula for the function α. The same general considerations hold true also, mutatis mutandis, for thermal effects and the function α'.

Now, among the different modifications proposed in [11] the first is the simplest one that is capable to yield the exact first two terms at high and low frequencies, and simultaneously, to automatically satisfy the condition on singularities, whatever the values of parameters ϕ, k_0, α_0, α_∞ and Λ (incidentally, this last nice feature of the formula is at variance to what was stated in this paper). Lafarge [12] expressed it in terms of the parameter α_0 and the same description was then immediately applicable, mutatis mutandis, to the thermal effects. The corresponding Pride-Lafarge's (PL) model formulae are[3]:

$$\alpha(\omega) = \alpha_\infty \left(1 + \frac{8}{MSt^2}\left(1 - p + p\sqrt{1 + \frac{M^2}{16p^2}St^2}\right)\right), \tag{29}$$

$$\alpha'(\omega) = 1 + \frac{8}{M'St'^2}\left(1 - p' + p'\sqrt{1 + \frac{M'^2}{16p'^2}St'^2}\right), \tag{30}$$

$$\beta(\omega) = \gamma - (\gamma - 1)/\alpha'(\omega), \tag{31}$$

where M and M' are as before, and p and p' are the new shape factors given by,

$$p = \frac{1}{\alpha_0 - \alpha_\infty}\frac{2k_0\alpha_\infty^2}{\phi\Lambda^2} \;\; ; \;\; p' = \frac{1}{\alpha_0' - 1}\frac{2k_0'}{\phi\Lambda'^2}. \tag{32}$$

It must be realized that, most probably, as long as the geometry is relatively simple, and as a side result of the strong constraints imposed by the special location of the singularities of the functions, these PL expressions constructed using the information of one more exact term than JA's at low frequencies, will also and more importantly, describe in a more accurate manner all of the viscous and thermal relaxation. They reduce to JA's if one replaces (32) by the simplifications $p = p' = 1$.

Now recall that in the frozen limit, as we have assumed a smooth pore-surface interface, our functions expand in successive powers of St^{-1} or St'^{-1} and the first two leading terms ($O(0)$ and $O(1)$) in these expansions are exactly described in terms of Johnson's and Allard's concepts of tortuosity α_∞ and characteristic lengths Λ and Λ'. We may try, using the improved but still approximate PL's Eqs. (29-32), to estimate the third $O(2)$ leading terms:

$$\alpha(\omega) = \alpha_\infty \left(1 + \frac{2}{St} + \frac{8(1-p)}{MSt^2} + O\left(\frac{1}{St^3}\right)\right), \tag{33}$$

$$\beta(\omega) = \gamma - (\gamma - 1)\left(1 + \frac{2}{St'} + \frac{8(1-p')}{M'St'^2} + O\left(\frac{1}{St'^3}\right)\right)^{-1}. \tag{34}$$

[3]Notice that in Ref. [13] there was a mistake of a factor 2 in the term under the root, without influence on further equations.

The second equation leads to[4] :

$$\beta(\omega) = 1 + (\gamma - 1)\left(\frac{2}{St'} + \frac{8(1-p')}{M'St'^2} - \frac{4}{St'^2} + O\left(\frac{1}{St'^3}\right)\right). \qquad (35)$$

Nevertheless, we should not hope that the above expansions yield anything precise as regards these third – model dependent – $O(2)$ terms. This is because the shape factors p and p' in the PL model (29-30) are not fixed through the "frozen" conditions, physical in this context, that Eqs. (33) and (35) should match the exact frozen limits, but instead, through the physically very different "relaxed" conditions that the relaxed limits Eqs. (17) should be verified. The example of cylindrical circular tubes may serve to illustrate this in quantitative manner.

2.3 The case of cylindrical pores

For a material with cylindrical circular pores of identical radius R (say for simplicity, all parallel and aligned along the direction of propagation), the two boundary value problems, Eqs. (2-4) and (6-7), determining $\alpha(\omega)$ and $\beta(\omega)$ are easily entirely stated and solved. In effect, these are nothing but the problems considered by Zwikker and Kosten [14] in simplifying (on account of the wide separation between wavelength and tube radius) the governing equations of the full Kirchhoff's theory of sound propagation in a cylindrical circular tube [15]. Thus, we may say that the conventional Equivalent-fluid theory (neglecting spatial dispersion and expressed by Eqs. (1-8)) is the direct generalization, to the case of arbitrary geometry, of the classical Zwikker and Kosten's theory. Now, Zwikker and Kosten's result is that $\alpha(\omega)$ and $\beta(\omega)$ express via Bessel functions as follows:

$$\frac{1}{\alpha(\omega)} = 1 - \chi(\omega) \;\; ; \;\; \beta(\omega) = 1 + (\gamma - 1)\chi(\omega\,\mathrm{Pr}), \qquad (36)$$

where $\chi(\omega)$ is the following relaxation function,

$$\chi(\omega) = \frac{2J_1\left((\frac{i\omega\rho_f}{\eta}R^2)^{1/2}\right)}{(\frac{i\omega\rho_f}{\eta}R^2)^{1/2}J_0\left((\frac{i\omega\rho_f}{\eta}R^2)^{1/2}\right)}, \qquad (37)$$

(going from relaxed value 1 at low frequencies to frozen value 0 at high frequencies). Using the known small-arguments and large-arguments series and asymptotic expansions of Bessel functions (or Kelvin functions), and comparing the results with those of the exact low-frequency and high-frequency limits (Eqs. (17) and (12)), the following parameters values are obtained:

$$k_0 = k_0' = \phi R^2/8 \;\; ; \alpha_0 = \alpha_0' = 4/3 \;\; ; \alpha_\infty = 1 \;\; ; \;\; \Lambda = \Lambda' = R. \qquad (38)$$

¿From Eqs. (28) and (32), the circular-tube shape factors M, p and M', p' are then identified as:

$$M = M' = 1 \;\; ; \;\; p = p' = 3/4. \qquad (39)$$

[4]Notice that in Ref. [13] the last term $-4/St'^2$ in Eq (35) was omitted.

In order to see the extent with which these values may be used to estimate the frozen $O(2)$ terms for the case at hand (aligned cylindrical circular pores), let us write for this case the known exact asymptotic high-frequency expansions:

$$\alpha(\omega) = 1 + \frac{2}{St} + \frac{3}{St^2} + O(\frac{1}{St^3}); \tag{40}$$

$$\beta(\omega) = 1 + (\gamma - 1)\left(\frac{2}{St'} - \frac{1}{St'^2} + O(\frac{1}{St'^3})\right). \tag{41}$$

If p and p' were fixed by the "frozen" conditions that the PL expansions (33) and (35) were to match the above exact expansions, they would be $p = p' = 5/8$. They are, however, fixed by other "relaxed" conditions, giving $p = p' = 3/4$. The difference (1/8) is not very large, but it produces a significant deviation on the $O(2)$ terms because of the factors of 8 in Eqs. (33) and (35). Thus for instance, with the values (39), the term St^{-2} in Eq. (33) has a coefficient equal to 2 instead of 3 in Eq. (40), while the term St'^{-2} in Eq. (35) has a coefficient equal to $-2(\gamma - 1)$ instead of $-1(\gamma - 1)$ in Eq. (41)[5]. These faulty PL coefficients, while significantly better than JA's (resp. 0 instead of 3 and $-4(\gamma - 1)$ instead of $-1(\gamma - 1)$), will obviously not yield accurate estimates of the exact $O(2)$ frozen terms. Here is a constitutive limitation of both models JA and PL that should be kept in mind. Its consequences on the time-domain Green functions will be illustrated later on.

3 Asymptotic $o(2)$ wave equation

The 1D wave equation that follows from Eqs. (1) is the following Helmholtz equation:

$$\frac{d^2p}{dx^2} + \omega^2 \frac{\rho_f \alpha(\omega)\beta(\omega)}{K_a} p = 0. \tag{42}$$

Using the PL high-frequencies asymptotic limits (33) and (35) we get,

$$\begin{aligned} \alpha(\omega)\beta(\omega)/\alpha_\infty = {} & 1 + \frac{2}{St} + (\gamma - 1)\frac{2}{St'} + \frac{8(1-p)}{MSt^2} + \\ & (\gamma - 1)\left(\frac{8(1-p')}{M'St'^2} - \frac{4}{St'^2} + \frac{4}{StSt'}\right) + o(2), \end{aligned} \tag{43}$$

and this is the form of the exact asymptotic result, except of course for the PL faulty values of p and p', if we intend to use Eqs. (32).

In the time domain, the corresponding asymptotic wave equation is written as follows:

$$\frac{\partial^2 p(x,t)}{\partial x^2} - A\frac{\partial^2 p(x,t)}{\partial t^2} - B\int_0^t \frac{\partial^2 p(x,t')/\partial t'^2}{\sqrt{t-t'}} dt' - C\frac{\partial p(x,t)}{\partial t} = 0. \tag{44}$$

[5] In Ref. [13] because the term $-4/St'^2$ in Eq (35) was omitted, the total coefficient of the term in St'^{-2} in Eq (35) was +2.

Comparison between (42-43) and (44) shows that the coefficients are given by:

$$A = \frac{1}{c^2} = \frac{\rho_f \alpha_\infty}{K_a}, \quad B = \sqrt{\frac{1}{\pi}} \frac{2}{c^2} \sqrt{\frac{\eta}{\rho_f}} \frac{1}{\Lambda} \left(1 + (\gamma - 1) \frac{\Lambda}{\Lambda' \sqrt{\mathrm{Pr}}} \right), \quad (45)$$

$$C = \frac{1}{c^2} \frac{\eta}{\rho_f} \frac{1}{\Lambda^2} m \ \text{ with} \quad (46)$$

$$m = \frac{8(1-p)}{M} + (\gamma - 1) \left[\frac{4\Lambda}{\Lambda' \sqrt{\mathrm{Pr}}} + \left(-4 + \frac{8(1-p')}{M'} \right) \frac{\Lambda^2}{\Lambda'^2 \, \mathrm{Pr}} \right]. \quad (47)$$

Again, this is the exact asymptotic $o(2)$ wave equation in time domain, except for a faulty value of the coefficient C, if we intend to use Eqs. (32). These equations are the equations (14-16) of Fellah et al. [13], who computed the Green function for an infinite medium described by this wave equation (44), by using the Laplace transform method[6]. We shall see in sections 4 and 5 that an alternative closed-form Green function may be obtained in simple manner for this same $o(2)$ asymptotic frozen limit. Before detailing this result, let us give the general definition of the Green function we employ.

4 A simple definition of a Green function and its asymptotic $o(1)$ and $o(2)$ frozen forms

4.1 Definition; scaled form

Another general method of defining and calculating a Green function in an infinite medium is by means of the effective frequency-dependent wavenumber k in this medium. Let us define our Green function $G(x,t)$ (or impulse response) as a propagated Dirac delta impulsive signal $\delta(t)$ imposed at $x = 0$, or more precisely, as the inverse Fourier transform of the propagation transfer function $G_\omega(x,\omega) = \exp(ikx)$:

$$G(x,t) = \int_{-\infty}^{\infty} \frac{d\omega}{2\pi} \exp\left[-i\omega t + ikx\right]. \quad (48)$$

Setting to zero the viscosity and thermal conduction coefficients, no frequency dispersion arises. The wavenumber writes $k = \omega/c$ where c, defined by the first Eq. (45), is the frozen speed of sound $c = c_f/\sqrt{\alpha_\infty}$. The Green function (48) coincides with a Dirac delta propagated at this velocity c: $G(x,t) = \delta(t - x/c)$.

Setting to nonzero values the viscosity and thermal conduction coefficients the medium wavenumber k writes,

$$k = \frac{\omega}{c} \sqrt{\frac{\alpha(\omega)\beta(\omega)}{\alpha_\infty}} = \frac{\omega}{c} \left[1 - h(St)\right], \quad (49)$$

making apparent a complex function $h(St)$ that describes frequency dispersion induced by the viscous and thermal relaxation processes. The Green function

[6] Nevertheless, coherent with Eq. (35), an additonal term has been included in the bracket of the coefficient C in Eq. (46) .

(48) writes,

$$G(x,t) = \int_{-\infty}^{\infty} \frac{d\omega}{2\pi} \exp\left[-i\omega(t - x/c) - i\frac{\omega}{c}h(St)x\right] \ . \tag{50}$$

This Green function $g_x(t - x/c) = G(x,t)$ now extends and flattens when observed at positions x more and more remote from the origin $x = 0$. Explicit asymptotic expressions of the Green's function defined in this manner will now be obtained by considering high-frequency asymptotic expansions of the wavenumber k (meaning high-frequency asymptotic expansions of the function h).

It will also be convenient to express these functions in scaled form, as functions of a dimensionless delay time τ and a dimensionless position variable ξ. To take but one example, before being Fourier-transformed, the Green function $G_\omega(x,\omega) = \exp(ikx)$ where k is – say – given by the model PL, may be viewed as a function of:

(i) one dimensionless frequency variable, e.g. $\Omega = \omega\Theta$ where Θ is the characteristic viscous relaxation time given by,

$$\Theta = \frac{\Lambda^2\rho_f}{\eta}, \tag{51}$$

(hence $St^2 = -i\Omega$),

(ii) one dimensionless position variable, e.g.

$$\xi = \frac{x}{c\Theta}, \tag{52}$$

(hence $\xi^{-1/2} = \Lambda\sqrt{\rho_f c/(x\eta)}$ can be regarded as a time domain Stokes number, when replacing $-i\omega$ by c/x in Eq. (22)).

(iii) a number of dimensionless parameters characteristic of the form of the porous space but not of its absolute dimensions (α_∞, M, p, M', p', and Λ'/Λ), and,

(iv) two dimensionless parameters characteristic of the fluid (γ and Pr).

Suppose that the parameters (iii) and (iv) of both the medium and the fluid are held constant. Function $G_\omega(x,\omega) = \exp(ikx)$ then reduces to a function of Ω which is parametrized by ξ. There follows that the shape of the corresponding time-domain function will depend, in scaled form, on ξ only, provided the time is counted in a dimensionless manner, e.g. for the time elapsed after the first arrival of the signal,

$$\tau = (t - \frac{x}{c})/\Theta. \tag{53}$$

But function $G(x,t)$ has the dimension of the inverse of time. Therefore,

$$\Theta G(x,t) = F_s(\xi,\tau), \tag{54}$$

with F_s a scale-invariant function that depends on the form of the pore space but not on its absolute dimensions:

$$F_s(\xi,\tau) = \int_{-\infty}^{\infty} \frac{d\Omega}{2\pi} \exp\left[-i\Omega\tau - i\Omega\xi h(\sqrt{-i\Omega})\right]. \tag{55}$$

4.2 Asymptotic $o(1)$'s and $o(2)$'s wavenumbers

4.2.1 General asymptotic result and PL asymptotic result

Recall that, since we assume a smooth pore-surface interface, in the frozen limit the product $\alpha(\omega)\beta(\omega)/\alpha_\infty$ expands in successive integral powers of St^{-1} (see footnote 1), hence giving the form:

$$k = \frac{\omega}{c}\left[1 + \frac{B_\omega}{\sqrt{-i\omega}} + \frac{C_\omega}{(-i\omega)} + o(2)\right]. \tag{56}$$

Constant c and B_ω are exactly given by:

$$\frac{1}{c} = \sqrt{\frac{\rho_f \alpha_\infty}{K_a}}, \quad B_\omega = 2\sqrt{\frac{\eta}{\rho_f}}\frac{1}{\Lambda} n_1 \quad \text{with} \tag{57}$$

$$2n_1 = 1 + (\gamma - 1)\frac{\Lambda}{\Lambda'\sqrt{\Pr}}, \tag{58}$$

whereas C_ω is a new unknown constant. We have been unable to find any rigorous theoretical statements that can be made about this coefficient. In the framework of the PL model it is estimated as (see Eq. (43)):

$$C_\omega = \frac{\eta}{\rho_f}\frac{1}{\Lambda^2} n_2 \quad \text{with} \tag{59}$$

$$2n_2 = \frac{8(1-p)}{M} - 1 + \frac{2(\gamma-1)\Lambda}{\Lambda'\sqrt{\Pr}} + \frac{(\gamma-1)\Lambda^2}{\Lambda'^2 \Pr}\left(\frac{8(1-p')}{M'} - 3 - \gamma\right). \tag{60}$$

However, for the reasons explained before, this is a rather loose determination. The relationships between these coefficients and the coefficients B and C are:

$$B_\omega = B\sqrt{\pi}c^2/2 \;\; ; C_\omega = (Cc^2 - B_\omega^2)/2. \tag{61}$$

In what follows $k_{o(1)}$ and $k_{o(2)}$ designate the asymptotic wavenumbers obtained by limiting the expansion of $\alpha(\omega)\beta(\omega)/\alpha_\infty$ to the first and second order exact frozen terms in St^{-1}:

$$k_{o(1)} = \frac{\omega}{c}\left[1 + \frac{B_\omega}{\sqrt{-i\omega}}\right], \tag{62}$$

$$k_{o(2)} = \frac{\omega}{c}\left[1 + \frac{B_\omega}{\sqrt{-i\omega}} + \frac{C_\omega}{(-i\omega)}\right]. \tag{63}$$

4.2.2 The case of cylindrical pores

For the case of cylindrical pores, using Eqs. (38) and (39), the expressions (57) and (59) of B_ω and C_ω become:

$$B_\omega = \frac{1}{R}\sqrt{\frac{\eta}{\rho_f}}\left(1 + \frac{\gamma-1}{\sqrt{\Pr}}\right); \;\; C_\omega = \frac{1}{R^2}\frac{\eta}{\rho_f} n_2; \; n_2 = \frac{1}{2} + \frac{\gamma-1}{\sqrt{\Pr}} - \frac{\gamma^2-1}{2\Pr}. \tag{64}$$

As expected, the last expression is not the exact one. This was given by

Keefe [17]:

$$n_2 = 1 + \frac{\gamma - 1}{\sqrt{\mathrm{Pr}}} - \frac{\gamma(\gamma - 1)}{2\,\mathrm{Pr}}. \tag{65}$$

For standard conditions in air, the exact result for n_2 in C_ω is 1.08, while the approximated one is 0.29, i.e. more than three times smaller. Notice that Johnson-Allard's model would give a negative estimate of -1.27 for it.

4.3 Frozen limit: Asymptotic $o(1)$'s and $o(2)$'s Green functions

Taking for k its asymptotic $o(1)$ expression (62) and making the inverse Fourier transform, it is a known result [20] that the corresponding analytical form of $G(x,t)$ is,

$$\begin{aligned} G_{o(1)}(x,t) &= 0 \text{ for } t < x/c, \\ G_{o(1)}(x,t) &= F_1(x,t) \text{ for } t > x/c, \end{aligned} \tag{66}$$

where

$$F_1(x,t) = \frac{1}{\sqrt{\pi}} \frac{Q(x)}{(t - x/c)^{3/2}} \exp\left[-\frac{Q^2(x)}{t - x/c}\right] \text{ , with } Q(x) = \frac{B_\omega x/c}{2}. \tag{67}$$

The dimension of the function $Q(x)$ is $\sqrt{t}$.

Likewise, taking for k its asymptotic $o(2)$ expression (63), it is also a known result of musical acoustics [18] that the corresponding analytical form of $G(x,t)$ is

$$\begin{aligned} G_{o(2)}(x,t) &= 0 \text{ for } t < x/c, \\ G_{o(2)}(x,t) &= F_1(x,t) \exp(-C_\omega x/c) \text{ for } t > x/c. \end{aligned} \tag{68}$$

Thus, it is demonstrated that, as regards the Green's functions, the effect of the second order terms on the inverse Stokes number (the effect of the term $C_\omega/(-i\omega)$ in the bracket (63)) is a pure multiplication by the factor $\exp(-C_\omega x/c)$: $G_{o(2)}(x,t) = G_{o(1)}(x,t)\exp(-C_\omega x/c)$. An expression (59) is given for the coefficient C_ω, but, as we have argued, it will not be an accurate expression if we put JA's values ($= 1$) or PL's values (32) of parameters p and p'. In general, the values p and p' that would give through (59) the exact value of parameter C_ω are unknown. They come from two new $o(2)$ frozen geometrical informations (let's say, the values p_∞ and p'_∞ of parameters p and p' in Eqs. (33) and (34), such that these expansions are exact) that are simply not present in the parameters introduced so far (ϕ, α_∞, Λ, Λ', k_0, k'_0, α_0, α'_0).

As examples of the scaling analysis, the formulae giving the $o(1)$ and $o(2)$ Green functions may be rewritten in the following scaled form:

$$\begin{aligned} \Theta G_{o(1)}(x,t) &= 0 \text{ for } \tau < 0, \\ \Theta G_{o(1)}(x,t) &= F_{s1}(\xi,\tau) \text{ for } \tau > 0, \end{aligned} \tag{69}$$

where,

$$F_{s1}(\xi,\tau)=\frac{1}{\sqrt{\pi}}\frac{n_1\xi}{\tau^{3/2}}\exp\left[-n_1^2\frac{\xi^2}{\tau}\right]\ \text{, with } 2n_1=1+(\gamma-1)\frac{\Lambda}{\Lambda'\sqrt{\mathrm{Pr}}}, \tag{70}$$

where n_1 is given by Eq. (58) and,

$$\begin{aligned}\Theta G_{o(2)}(x,t) &= 0 \text{ for } \tau<0,\\ \Theta G_{o(2)}(x,t) &= F_{s1}(\xi,\tau)\exp(-n_2\xi) \text{ for } \tau>0,\end{aligned} \tag{71}$$

where n_2 is given by Eq. (60).

4.4 Relaxed limit: Asymptotic diffusive Green function

The (relaxed) purely diffusive Green function G_{diff} can be obtained by assimilating $\beta(\omega)$ with γ and $\alpha(\omega)$ with its first leading term $\eta\phi/(-i\omega\rho_f k_0)$ in Eq. (17). In the relaxed d.c. approximation where $\beta=\gamma$ and $\alpha=\eta\phi/(-i\omega\rho_f k_0)$, one finds that the wavenumber expands as,

$$k=k_{diff}=\frac{1}{c}\left(\frac{8\gamma}{M\Theta}\right)^{1/2}\sqrt{i\omega}. \tag{72}$$

(we have used the relation (24)). Formally, this is the form (62) with, in the first term, c replaced by ∞, and, in the second term, B_ω/c replaced by the factor before $\sqrt{i\omega}$. Straightforward calculations using the solution (66-67) and the following dimensionless time ((53) with $c=\infty$ and a prime to avoid confusion)

$$\tau'=t/\Theta, \tag{73}$$

then show that,

$$\begin{aligned}\Theta G_{diff}(x,t) &= 0 \text{ for } \tau'<0\\ \Theta G_{diff}(x,t) &= F_{s,diff}(\xi,\tau') \text{ for } \tau'>0,\end{aligned} \tag{74}$$

where,

$$F_{s,diff}(\xi,\tau')=\frac{1}{\sqrt{\pi}}\sqrt{\frac{2\gamma}{M}}\frac{\xi}{\tau'^{3/2}}\exp\left[-\frac{2\gamma}{M}\frac{\xi^2}{\tau'}\right]. \tag{75}$$

5 FFT computations of Green's functions

In addition to the previous asymptotic analytic Green's functions, full Green's functions $G(x,t)$ computed numerically by inverse FFT (Fast Fourier Transform) of the transfer function $\exp(ikx)$, can always be obtained as soon as exact or approximate full-frequency expressions of the wavenumber k in Eq. (49) are known. These FFT computations are to be carefully done, however, as it is detailed below.

For the case of arbitrary porous media, approximate models such as JA or PL may be used for $k(\omega)$, leading to the computation by FFT of approximate Green functions $G(x,t)$. For the case of simple workable geometries (e.g., cylindrical circular aligned pores of identical radius) exact expressions are available

(e.g., Zwikker and Kosten's), leading to the computation by FFT of exact Green functions $G(x,t)$.

In section 6 we shall study particularly, in the case at hand of cylindrical circular pores, the relationships between the different, asymptotic or not, approximate or exact, Green's functions. For later use, it will be convenient to distinguish and denote respectively by:

G the exact (Zwikker and Kosten) Green function;

G_{JA} the full JA Green function ($p = p' = 1$);

G_{PL} the full PL Green function ($p = p' = 3/4$);

G_{mPL} the modified full PL Green function (defined by PL's expressions with $p = p' = 5/8$);

An important point is that the diffusion solution G_{diff} (Eq. (74)) is used in our FFT computations to improve the accuracy of calculations. Indeed, instead of calculating directly the inverse Fourier transform $G(x,t)$ of the function $\exp(ikx)$, we first compute the inverse Fourier transform $G'(x,t)$ of the function $\exp(ikx) - \exp(ik_{diff}x)$ (the latter difference being smoothly varying at low frequencies and rapidly decreasing at high frequencies), and next use the relation $G(x,t) = G'(x,t) + G_{diff}(x,t)$, with $G_{diff}(x,t)$ as given by the Eqs. (73-75) above (see Ref. [22]). The validity of the FFT computation has been checked for first order asympotic expression, with an accuracy better than 1%.

The FFT computations can be compared with the following expressions:

$G_{o(1)}$ the (frozen) $o(1)$ Green function;

$G_{o(2)}$ the (frozen) $o(2)$ Green function ($p = p' = 5/8$);

$G_{JAo(2)}$ the JA $o(2)$ Green function ($p = p' = 1$);

$G_{PLo(2)}$ the PL $o(2)$ Green function ($p = p' = 3/4$).

With $p = p' = 5/8$, $p = p' = 1$, and $p = p' = 3/4$, the above expression (71) yields the Green functions $G_{o(2)}(x,t)$, $G_{JAo(2)}(x,t)$, and $G_{PLo(2)}(x,t)$, respectively.

Finally, the FFT computations can be compared to the solution of the asymptotic o(2) wave equation (44), for both cases $p = p' = 5/8$ and $p = p' = 3/4$ (we choose to compute the solutions using FFT):

$G_{WEo(2)}$ the (frozen) $o(2)$ Green function ($p = p' = 5/8$);

$G_{WEPLo(2)}$ the PL $o(2)$ Green function ($p = p' = 3/4$).

These solutions being of $o(2)$ as well as the solutions using the asymptotic $o(2)$ wavenumber are expected to be very close to the latter.

6 Computed results

For the computation, the values of the parameters have been chosen close to those of material M1 in Ref. [13]. The porosity is $\phi = 0.82$, the flow resistivity $\sigma = 196000 Nm^{-4}s$, the permeability $k_0 = \eta/\sigma = 9.225\ 10^{-11} m^2$, corresponding to a radius $R = 3\ 10^{-5} m$. The temperature is $20°C$, and the Prandtl number $\mathrm{Pr} = 0.71$. The characteristic viscous relaxation time is $\Theta = 6.10^{-5} s$.

6.1 Time responses

The chosen length is $5.3mm$ (the dimensionless length is $\xi = 0.3152$). Fig. 1 shows the results for the dimensionless Green function, obtained by FFT. The Pride-Lafarge description is compared with the exact Zwikker and Kosten

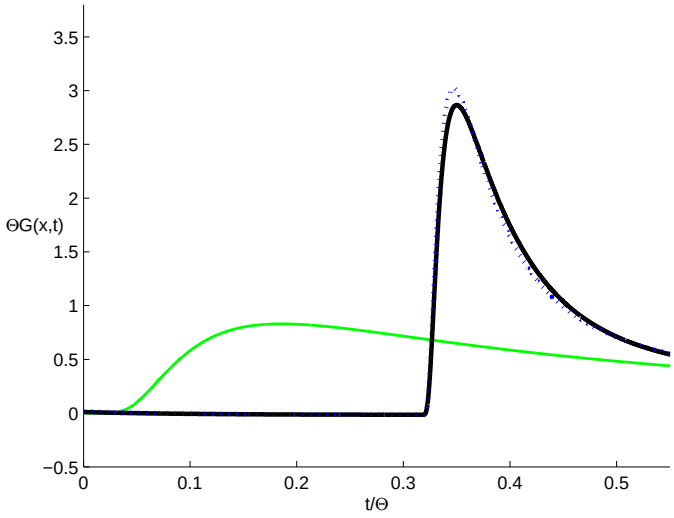

Figure 1: Green function $\Theta G(x,t)$ with respect to time t/Θ (both are dimensionless). (Black), solid line: Zwikker and Kosten formula (Eqs. (36) and (37). (Blue), dotted line Pride Lafarge description (Eqs. (29) to (32)). (Green), thin, solid line: diffusive limit (Eqs. (74) and (75)). For very long times, the diffusive limit is reached.

formula. As expected, the full PL description is very satisfactory for short times (high frequencies) and long times (low frequencies). For very long times, both descriptions reach the diffusive (analytical) limit, i.e. the Poiseuille behavior is reached.

In order to precise these results, Fig. 2 shows a zoom of the previous figure, and other approximations have been added. The modified PL Green function, denoted G_{mPL}, can be compared to the PL Green function. As expected, it is more accurate for short time (during the signal rise) than the non modified PL function, but it is less accurate for long times, because the choice of the parameters p and p' has been done from the frozen limit expressions instead of the relaxed limit expressions. Otherwise the JA model yields less accurate results than both PL models. Notice that $G_{o(2)}$, the (frozen) $o(2)$ Green function ($p = p' = 5/8$), which is a very simple analytical expression, leads to interesting results, except at long times. This will be confirmed by the calculation presented hereafter.

6.2 Maximum values of the time response

The previous results are concerned with a fixed value of the parameter ξ , i.e. a fixed value of the thickness of the material layer. In order to compare the different descriptions for several values of ξ, we chose to compare the maximum values of the time responses (there is a unique maximum). It is noticeable that for the asymptotic (frozen) expressions at the first order, F_{s1}, the maximum value and the corresponding time $\tau_{\max}$ are given by an analytical expression,

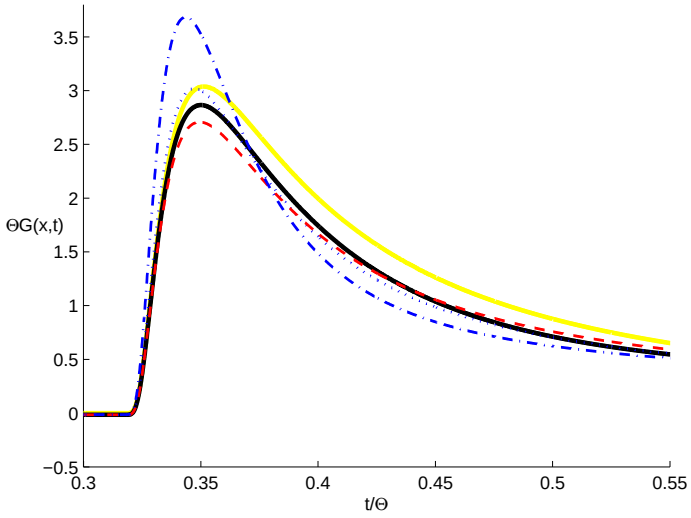

Figure 2: Green function $\Theta G(x,t)$ with respect to time t/Θ (zoom of figure 1). (Black), solid line: Zwikker and Kosten formula; (blue), dotted line: PL formula; (red), dashed line PL modified formula; (blue), mixed line: JA formula; (yellow), solid, pale line: frozen o(2)'s Green function $G_{o(2)}$.

obtained from Eq. (70):

$$\begin{aligned} Max(F_{s1}) &= \frac{1}{\sqrt{\pi}}\left[\frac{3}{2}\right]^{3/2} e^{-(3/2)}\frac{1}{n_1^2\xi^2} = \frac{0.2312}{n_1^2\xi^2}\ ; \\ \tau_{\max} &= \frac{2}{3}n_1^2\xi^2. \end{aligned}$$

For the asymptotic expression of order 2, the time $\tau_{\max}$ remains the same, while the maximum needs to be corrected from order 1 by the factor $\exp(-n_2\xi)$, according to Eq. (71). Fig. 3 shows the result for the exact Green function G and the two PL models, G_{PL} and G_{mPL}, as well as the diffusive function G_{diff}. It shows the neperian logarithm of the maximum value of F_s with respect to the dimensionless space variable ξ. The two PL models seem to be very good; however we prefer to give more insight by subtracting the result corresponding to the exact Green function, as shown in Fig. 4. As expected, the PL description is very good for high distances ξ, while the modified PL description is better for small distances ξ. Otherwise both are better than the JA description. In order to make possible a comparison with the asymptotic solutions (presented hereafter in Fig. 5), the best asymptotic solution is shown in Fig. 4. It is bad for large distances. The transition range values of the distance ξ is approximately between 0.036 and 1.7, corresponding to a range for the time domain Stokes number $5.3 \geq \xi^{-1/2} \geq 0.75$. This range is similar to that accepted for the frequency domain Stokes number defined by Eq. (22) (see e.g. Ref. [17]).

Fig. 5 shows that the PL description is slightly better than the first order of the frozen asymptotic, but the second order of the frozen asymptotic is the

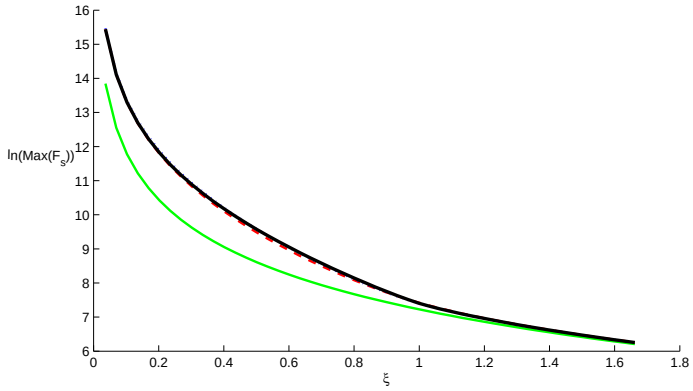

Figure 3: Neperian logarithm of the Green function maximum. (Black) solid, thick line: exact Green function G. (Blue) dotted line: PL Green function G_{PL}. (Red), dashed line: modified Green function G_{mPL}. (Green) solid, thin line: diffusive Green function, G_{diff}.

best approximation. Otherwise, for short distances ξ, the second order of the asymptotic wave equation WE exhibits the expected convergence to the results of the solution based on wavenumber expansion at second order, for both the coefficients obtained from the Zwikker and Kosten solution ($p = p' = 5/8$) and those of the PL model ($p = p' = 3/4$). Nevertheless, for higher distances, the asymptotic WE solution seems to be slightly less accurate than the asymptotic wavenumber solution: it is not easy to have an interpretation for this result.

7 Conclusion

For very short dimensionless distances, the value of the time maximum is inversely proportional to the square of the distance, but when the distance increases, the decrease becomes exponential. This behavior is correctly represented by the second order of the frozen asymptotic. Nevertheless, if the coefficient of the second order is known for some geometries, such as for cylindrical pores, it is not known in general. The PL description remains the more satisfactory for the general case, but it gives faulty description of the exponential decreasing, because the coefficients p and p' are determined from the relaxed limit. The different figures presenting the results for dimensionless quantities can help for the choice of certain approximations.

The second order solution of the wave equation, as presented in Ref. [13] differs (by definition) by the third order with the solution based on wavenumber expansion at second order, the latter being simpler to use in practice. Looking at the calculation made in the frequency domain, the figure 3 of this paper exhibits a ratio between the PL description and the JA one (with $p = p' = 1$) that is almost independent of frequency: this is confirmed by the asymptotic calculation of the wavenumber (Eq. (71)).

A problem of major interest is the use of the present investigation for the inverse problem, i.e. the determination of the parameters of a given material.

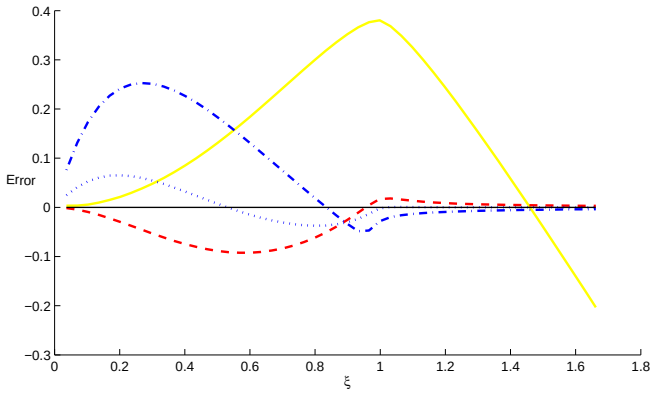

Figure 4: Error on the neperian logarithm of the Green function maximum. The different solution are compared to the exact one, the error being the difference between the corresponding value and the eaxct value. (Blue) dotted line: G_{PL}. (Red), dashed line: modified PL G_{mPL}. (Blue) mixed line: G_{JA}. (Yellow) solid line: frozen o(2) Green function $G_{o(2)}$.

In this connection we have illustrated in this paper by direct FFT a simple fact. This fact is that the description of the time domain Green functions may be significantly improved by employing the full model expressions (instead of the asymptotic expressions). It suggests therefore that there is still a strong potential of improvement of the inverse methods of characterization based on recording transmitted and reflected pulses on different thicknesses of a material, provided the full expressions are exploited in the analysis.

Assuming that we are dealing here with sufficiently well-defined and reproducible materials, we may suggest moreover, that this potential may be difficult to exploit fully, within the framework of current models including the most precise PL. Indeed, the present work has highlighted one fundamental limitation of these models. It has shown that, even if it would be possible to gain precise experimental information on the unknown geometrical coefficients determining the high-frequency "second order" attenuation effect, it would not be possible to properly exploit this information in the framework of the current models. It is thus possible that working in the framework of a new model free from the highlighted limitation would present significant advantages for the precise inversion. These questions would have to be considered in further work.

Acknowledgments

We wish to thank Bruno Lombard for fruitful discussions.

References

[1] D.L. Johnson, J. Koplik, R. Dashen, Theory of dynamic permeability and tortuosity in fluid-saturated porous media, J. Fluid Mech. 176 (1987) 379–

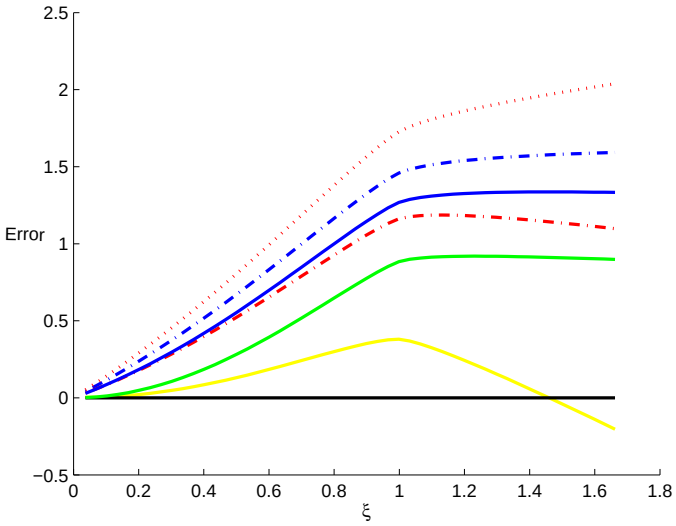

Figure 5: Error on the neperian logarithm of the Green function maximum. The different asymptotic solutions are compared to the exact one, the error being the difference between the corresponding value and the exact value. ¿From the largest to the smaller error, the following curves represent respectively: $G_{JAo(2)}$; $G_{o(1)}$; $G_{WEPLo(2)}$; $G_{PLo(2)}$; $G_{WEo(2)}$; $G_{o(2)}$, the latter being also shown in Fig. 4.

402.

[2] D.L. Johnson, J. Koplik, L.M. Schwartz, New pore-size parameter characterizing transport in porous media, Phys. Rev. Lett. 57 (1986) 2564-2567.

[3] M.Y. Zhou, P. Sheng, First principles calculations of dynamic permeability in porous media, Phys. ReV. B 39 (1989) 12027-12039.

[4] H. Darcy, Les fontaines publiques de la ville de Dijon, V. Dalmont, Paris, (1856)

[5] A. Cortis, D. Smeulders, J.-L. Guermond, D. Lafarge, Influence of pore roughness on high-frequency permeability, Phys. Fluids 15 (2003) 1766–1775.

[6] M. Avellaneda, S. Torquato, Rigorous link between fluid permeability, electrical conductivity, and relaxation times for transport in porous media, Phys. Fluids A 3 (1991) 2529-2540.

[7] A.N. Norris, On the viscodynamic operator in Biot's equations of poroelasticity, J. Wave Mat. Interact. 1 (1986) 365-380.

[8] J.F. Allard, Propagation of Sound in Porous Media: Modeling Sound Absorbing Materials, Chapman and Hall, London, 1993.

[9] D. Lafarge, P. Lemarinier, J.F. Allard, V. Tarnow, Dynamic compressibility of air in porous structures at audible frequencies, J. Acoust. Soc. Am. 102 (1997) 1995–2006.

[10] Y. Champoux, J.F. Allard, Dynamic tortuosity and bulk modulus in air-saturated porous media, J. Appl. Phys. 70 (1991) 1975-1979.

[11] S.R. Pride, F.D. Morgan, A.F. Gangi, Drag forces of a porous-medium acoustics, Phys. Rev. B (1993) 4964–4978.

[12] D. Lafarge, Sound propagation in porous materials having a rigid frame saturated by gas, (in French). Ph.D. Dissertation, Université du Maine, 1993.

[13] Z.E.A. Fellah, C. Depollier, M. Fellah, W. Lauriks, J.-Y. Chapelon, Influence of dynamic tortuosity and compressibility on the propagation of transient waves in porous media, Wave motion 41 (2005) 145-161.

[14] C. Zwikker, C.W. Kosten, Sound Absorbing Materials, Elsevier, New York, 1949.

[15] G. Kirchhoff, Uber des Einfluss der Wärmeleitung in einem Gase auf die Schallbewegung, Annalen der Physik and Chemie 134 (1868) 177-193.

[16] H. Tijdeman, On the propagation of sound waves in cylindrical tubes, J. Sound Vib. 39 (1975) 1–33.

[17] D. H. Keefe, Acoustical wave propagation in cylindrical ducts: Transmission line parameter approximations for isothermal and nonisothermal boundary conditions, J. Acoust. Soc. Am. 75 (1984), 58-62.

[18] J. D. Polack, X. Meynial, J. Kergomard, C. Cosnard and M. Bruneau, Reflection function of a plane sound wave in a cylindrical tube, Revue Phys. Appl. 22 (1987) 331-337.

[19] D. Lafarge, The equivalent fluid model, in Materials and Acoustics Handbook, M. Bruneau and C. Potel eds, ISTE-Wiley, London, 2009, pp 205-228.

[20] L.D. Landau, E. Lifshitz, Fluid Mechanics, Vol. 6 (2nd ed.), Butterworth-Heinemann, 1987.

[21] L.D. Landau, E. Lifshitz, Electrodynamics of continuous media, Elsevier Butterworth-Heinemann, 2006.

[22] J. Kergomard, J.D. Polack, J. Gilbert, Propagation speed of a plane impulsive wave in a sound tube (in French), J. Acoustique 4 (1991),467-483.